Stable emission and fast optical modulation of quantum emitters in boron nitride nanotubes

Jonghoon Ahn,[1,†] Zhujing Xu,[2,†] Jaehoon Bang,[1] Andres E. Llacsahuanga Allcca,[2]
Yong P. Chen,[1,2,3,4] and Tongcang Li[1,2,3,4,*]

[1]School of Electrical and Computer Engineering, Purdue University, West Lafayette, Indiana 47907, USA
[2]Department of Physics and Astronomy, Purdue University, West Lafayette, Indiana 47907, USA
[3]Purdue Quantum Center, Purdue University, West Lafayette, Indiana 47907, USA
[4]Birck Nanotechnology Center, Purdue University, West Lafayette, Indiana 47907, USA
*Corresponding author: tcli@purdue.edu

Atom-like defects in two-dimensional (2D) hexagonal boron nitride (hBN) have recently emerged as a promising platform for quantum information science. Here, we investigate single-photon emissions from atomic defects in boron nitride nanotubes (BNNTs). We demonstrate the first, to the best of our knowledge, optical modulation of the quantum emission from BNNTs with a near-infrared laser. This one-dimensional system displays a bright single-photon emission, as well as high stability at room temperature, and is an excellent candidate for optomechanics. The fast optical modulation of a single-photon emission shows multiple electronic levels of the system and has potential applications in optical signal processing. © 2018 Optical Society of America

Single-photon emitters (SPEs) are playing a key role in the route toward future quantum technologies such as quantum communication and quantum computing. Many solid-state SPEs have been explored, including quantum dots, carbon nanotubes, two-dimensional (2D) materials, and color centers in crystals [1]. They show potential in on-chip fabrication and integration, which enables scalable structure for quantum information processing. Recently, ultra-bright SPEs from point defects in 2D hexagonal boron nitride (hBN) with mono- and multilayers were discovered [2]. As a well-suited platform for room-temperature quantum emissions, 2D hBN has attracted a plethora of studies, including photoluminescence spectra distributed over a wide range [3–7], stable quantum emissions at up to 800 K [4,8], and other properties [2,9–12]. Moreover, a recent work reported a single-photon emission from bundles of boron nitride nanotubes (BNNTs) with an average diameter of 5 nm [13]. It reports bleaching under 532 nm excitation and notes the bleaching can be alleviated with N, N′-Dimethylacetamide (DMAc) solutions and indium tin oxide (ITO) substrates [13].

BNNTs can simply be seen as rolled boron nitride sheets [14,15]. They are structurally similar to carbon nanotubes, but have a wide bandgap (5.95 eV) and high thermal and chemical stabilities [15]. With these features, BNNTs emerge as a natural candidate for nanotube-based nanodevices and protective shields, especially in hazardous and extreme environments [16]. Compared to 2D hBN, a BNNT will allow us to explore the effects of dimension and curvature on the quantum emitters embedded inside. The optically active SPEs in low dimensions will also open up opportunities in quantum technologies with opto-mechanical resonators or other hybrid systems [17–21].

In this work, we identify and study single-photon emissions from point defects in BNNTs with an average diameter of 50 nm. Thanks to their intrinsic curvature, 50-nm-diameter BNNTs host abundant SPEs compared to 2D hBN. We observe that their SPEs are much more stable than those in bundles of 5-nm-diameter BNNTs. Finally, we implement optical modulation of the fluorescence from the BNNTs by applying a near-infrared (NIR) laser with a wavelength of 1064 nm.

We use a home-built confocal microscope to selectively excite point defects in the 50-nm-diameter BNNTs as shown in Fig. 1(a). We dilute a commercial BNNT powder in an ethanol solution and disperse it on a glass slide. The color centers are pumped to the excited state with a 300 μW 532 nm continuous-wave (CW) laser focused through an air objective lens with an NA of 0.9. The fluorescence [shown in orange in Fig. 1(a)] is collected with the objective lens and is guided to the single-photon counters and a spectrometer. For the optical modulation of the photon emissions, an additional 1064 nm laser (shown in red) is superimposed onto the 532 nm beam, and the power is controlled with an acousto-optic modulator (AOM). Figure 1(b) presents an SEM image of the BNNTs. The SEM image confirms that the nanotubes have an average diameter of approximately 50 nm and the nanotubes are well separated. Figure 1(c) presents the Raman scattering spectrum of the BNNTs. The Raman shift here is 1369 cm^{-1}, which agrees well with the results of earlier studies [2,7,9,15,22].
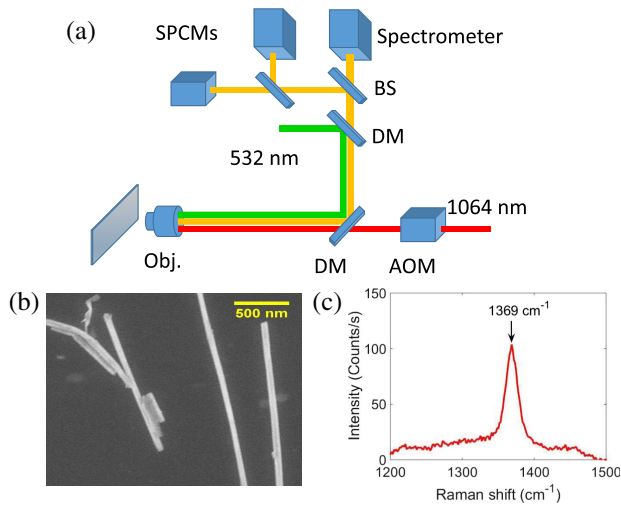
Fig. 1. (a) Simplified schematic of the experiment (SPCMs, single-photon counting modules; BS, beam splitter; DM, dichroic mirror; Obj, objective lens; AOM, acousto-optic modulator). A green laser ($\lambda = 532$ nm) is used to excite defects in BNNTs on a glass slide. The emitted fluorescence (shown in orange) is collected with the objective lens (NA = 0.9), and detected by two photon counters and a spectrometer. A NIR laser ($\lambda = 1064$ nm) is used for optical modulation. (b) A scanning electron microscope (SEM) image of the BNNTs. The diameter of nanotubes is approximately 50 nm. (c) A Raman spectrum of a BNNT. The Raman shift is 1369 cm^{-1}.

Figure 2 displays different characteristics of the quantum emitters recorded from the BNNTs at room temperature. The camera images are collected from back reflection under white light and the results are displayed in Figs. 2(a) and 2(b). We notice that some parts of the nanotubes are arched, rather than being completely attached to the substrate surface. The nanotubes with a bent structure tend to have more defects.
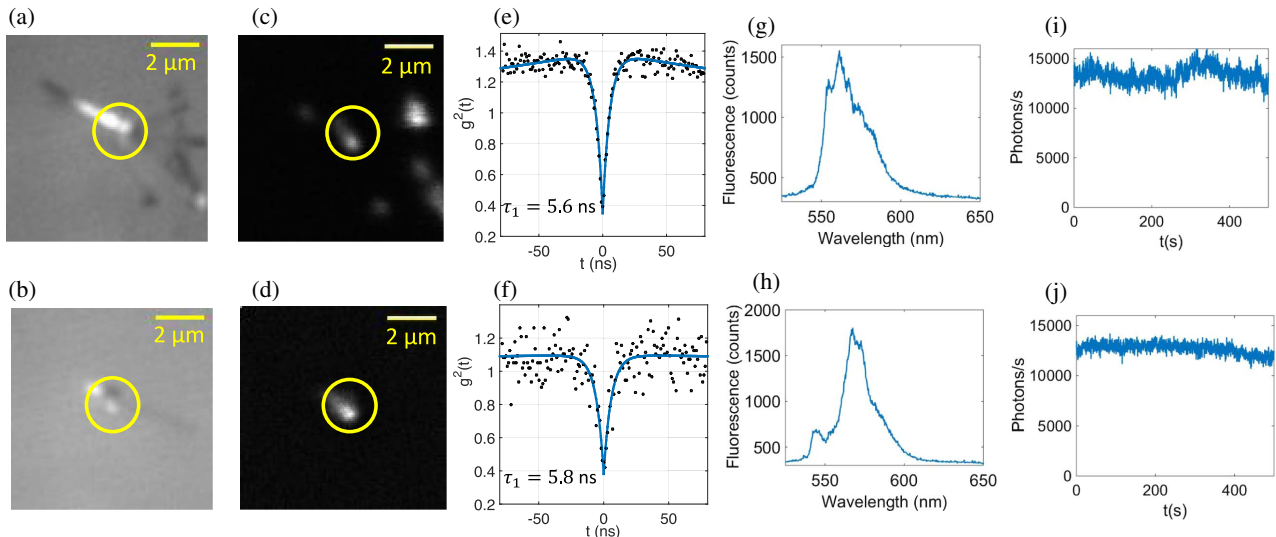
The confocal images [Figs. 2(c) and 2(d)] are taken by collecting the fluorescence from the defects excited with a 532 nm sub-bandgap pump laser.

To demonstrate that the collected signal in the confocal photoluminescence map comes from a SPE, we measure the second-order autocorrelation functions $g^2(\tau)$ using a Hanbury Brown and Twiss interferometry setup. The results are shown in Figs. 2(e) and 2(f). Both autocorrelation curves show $g^2(0) < 0.5$, proving that both point defects are SPEs. The autocorrelation functions were fit by a three-level model [2,23,24],

$$g^2(\tau) = 1 - (1 + a)e^{(-|\tau|/\tau_1)} + ae^{(-|\tau|/\tau_2)}, \quad \text{(1)}$$

where parameters τ_1 and τ_2 are the lifetimes of the excited state and the metastable state, respectively. a is the fitting parameter. From the first emitter, we obtain $g^2(0) = 0.35$ and the fluorescence lifetimes extracted from the fitting of the $g^2(\tau)$ curve are $\tau_1 = 5.6$ ns and $\tau_2 = 250.3$ ns. The other emitter has $g^2(0) = 0.38$, with the fitting yield lifetimes of $\tau_1 = 5.8$ ns and $\tau_2 = 321.3$ ns. The fluorescence lifetime varies among different samples possibly due to local strains in the BNNTs. In addition, the diameter of the BNNTs is much smaller than the wavelength of the excitation laser, which may cause nano-antenna effects that affect the lifetimes [13,25]. Nevertheless, considering the uncertainty in the fittings, the measured lifetimes are consistent with the results for SPEs in hBN monolayers [2].

For characterization of the defect, we record the photoluminescence spectra of each quantum emitter [presented in Figs. 2(g) and 2(h)]. Both emitters have broad features and asymmetric line shapes in the spectra. These could be due to phonons in the nanotubes and background emissions. The peaks for the two emitters are found at 571 nm and 569 nm, respectively, presumably attributed to the zero phonon line (ZPL) of the defects. Based on the ZPL classification defined in [3], the defects in our BNNTs belong to Group 1 and the fluorescence agrees well with the features of the spectra.

Fig. 2. (a) and (b) Camera images under white light for two different defects in different BNNTs. Yellow circled regions indicate the positions of the defects. (c) and (d) Confocal photoluminescence map of the color centers under the 532 nm excitation. (e) and (f) The measured second-order autocorrelation functions of the two color centers. $g^2(0) < 0.5$ is satisfied in both cases, which proves that they are SPEs. (g) and (h) Measured spectral features of two color centers with a 550LP filter. (i) and (j) Photon emission rate as a function of time for 500 s, which demonstrates the stability of the point defects.

A previous study on bundles of BNNTs with an average diameter of 5 nm reported obvious bleaching under 532 nm excitation and it used DMAc solutions and ITO substrates to resolve bleaching [13]. On the contrary, in our experiment, we simply dilute the commercial 50 nm BNNTs in an ethanol solution and disperse them on a glass slide. The single-photon emissions from our sample are stable for over 20 min under the 532 nm excitation. We notice that some parts of the nanotubes are arched in air instead of being adhered onto the substrate. Stable photon emissions are also observed in those arched sections. Therefore, in our sample, we surmise that the stability of the emission has little to do with the substrate material. To investigate the stability of the point-like defects in BNNTs, we maintain a constant pumping beam and track the photon number for 500 s as shown in Figs. 2(i) and 2(j). We find that the photon numbers vary less than 20% for 500 s, which proves the stability of photon emissions [2,7,8]. For comparison, we have also conducted experiments on BNNT samples with an average diameter of about 5 nm under the same condition on both ITO and glass substrates. It is much more difficult to find a SPE and the emissions are very unstable under the 532 nm illumination. Most of them bleach within 10 s. This is consistent with former results [13] and is likely due to a much larger curvature in 5-nm-diameter BNNTs.

For further advancements in photonic devices and quantum signal processing with SPEs, realization of optical transistors has been pursued and implemented in several systems. Previously, optical transistors have been realized in several systems, including photonic crystals [26], optomechanical resonators [27], single molecules [28], and single nitrogen-vacancy (NV) centers in nanodiamonds [29]. Similar to NV centers in nanodiamonds, SPEs in hBN have been proved to be stable at room temperature, but their energy levels are still an open question. Several theories and calculations of possible energy levels are available based on the measured spectra and the fluorescence signal [2,3,5,6,11,12,30]. The optical modulation of SPEs in BNNTs with a NIR laser will not only create optical transistors but can also provide additional information about the possible energy levels of SPEs in BNNTs. We perform the optical modulation of SPEs in the same 50 nm diameter BNNT sample deposited on a glass slide. An additional 1064 nm laser beam is superimposed onto the excitation laser for the modulation of the photon emission. Figure 3(a) shows the schematics for the optical modulation of BNNTs, similar to the scheme for the NV centers of nanodiamonds in [29]. With a CW 532 nm pump laser, the point defect in BNNTs shows stable fluorescence as shown in Figs. 2(i) and 2(j). Simultaneously, the non-resonant NIR laser is applied and drives the excited state to the dark state. Therefore, the NIR beam serves as a control laser, which reduces the fluorescence signal from the quantum emitters. Furthermore, controlled with an AOM, the NIR beam is modulated to a square pulse shown in red in Fig. 3(a), and the number of the emitted photons from the color center follows an opposite pattern, which is shown in orange.

To begin, we examine the pulse shape of the 1064 nm laser controlled with the AOM as shown in Fig. 3(b). The total span of the recorded data is 20 μs, while the modulated square pulse has a period of 5 μs. The pulse shape here is described by the number of photons collected from the back reflection and is normalized. Due to background noise, the measured minimum amplitude for the pulse is not zero.

Next, we investigate the effect of the NIR illumination on the fluorescence from the color centers in the BNNTs. For the excitation, a 532 nm pump beam with a constant power of 300 μW is used and the maximum power of the 1064 nm gating laser is 800 mW before the objective lens. The time-resolved fluorescence from the BNNTs is measured by continuous tracking of the photon numbers received at
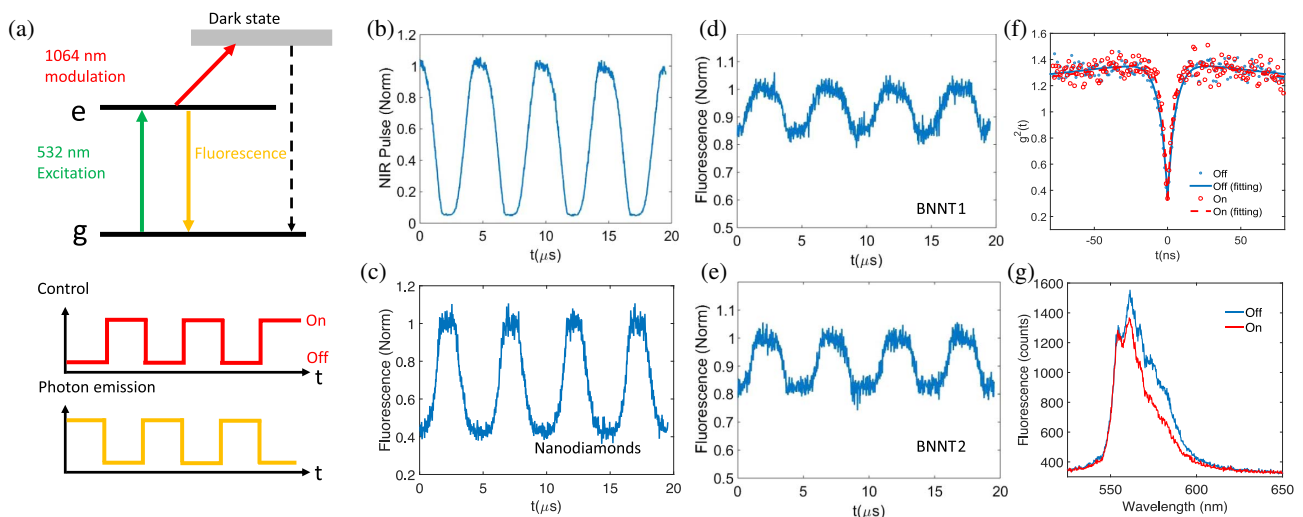

Fig. 3. Optical modulation of photon emission from BNNTs under NIR illumination. (a) Schematic demonstration of the optical switching. The 1064 nm laser, acting as the control signal (in red), is applied on top of the 532 nm beam (in green). The photon emission signal (in orange) represents the fluorescence from BNNTs and is modulated by the control signal. (b) The pulse shape of the 1064 nm laser. (d) and (e) By controlling the power of the 1064 nm laser with an AOM, we get the optical modulation of the fluorescence from two different BNNT single color centers. BNNT1 and BNNT2 correspond to the two color centers in Fig. 2. (c) For comparison, the same condition is applied to NV centers in a nanodiamond. (f) The measured second-order autocorrelation functions of BNNT1 and its curve fitting when the 1064 nm control laser is on (in red) and off (in blue). (g) The measured spectrum of BNNT1 when the 1064 nm control laser is on (in red) and off (in blue). Other conditions are the same. The slight decrease of fluorescence is caused by the modulation from the control laser.

the single-photon counter. With the modulated NIR laser and the constant green laser, we observe obvious modulation of the fluorescence evolution in BNNT SPEs, which are demonstrated in Figs. 3(d) and 3(e). Here, BNNT1 and BNNT2 correspond to the two SPEs in Fig. 2. For comparison, we repeat the procedures above with NV centers in nanodiamonds with an average diameter of 40 nm. The powers used for the green and NIR lasers are the same as above. Figure 3(c) shows the optical modulation of NV centers in a nanodiamond. In our system, we were able to achieve up to 60% modulation of a NV center fluorescence, which is comparable to the 80% modulation reported in [29]. The BNNTs, on the other hand, showed an optical modulation of 10%–20%. The lower modulation depth may be attributed to the shorter lifetime of the excited state $|e\rangle$ in BNNTs [3,31]. The excited state of NV$^-$ in nanodiamonds has an average lifetime of about 20 ns [32], while the measured lifetime in BNNTs is around 5 ns. Therefore, the fluorescence process is much faster in BNNTs than that of NV centers in nanodiamonds. Because of the shorter lifetime of the excited state $|e\rangle$ in BNNTs, it will be more difficult to pump it from $|e\rangle$ to the dark state with a NIR laser. Meanwhile, the quantum emission in BNNTs should have a shorter response time and, accordingly, a faster optical modulation. However, in our current experimental system, the modulation speed is limited by the response time of our AOM, which is about 1 μs.

Additionally, we also measure the optical properties of the SPEs when the control laser is on. The comparison of the $g^2(t)$, as well as the spectrum of BNNT1, when the 1064 nm laser is on and off is shown in Figs. 3(f) and 3(g). The blue dots and red hollow circles in Fig. 3 represent the measured $g^2(t)$ when the 1064 nm control laser is off and on, respectively. The $g^2(t)$ only changes slightly when the control laser with a large power of 800 mW is on or off, which verifies the stability of single-photon emissions from BNNTs. The spectrum of BNNT1 when the 1064 nm laser is off is shown in the blue solid line in Fig. 3(g), while the red solid line represents the spectrum when the 1064 nm laser is on. There is a decrease in the fluorescence, which agrees with the modulation shown in Fig. 3(c).

In conclusion, we investigate the quantum emission from BNNTs. Results prove that BNNTs with a diameter of about 50 nm are a platform for stable SPEs at room temperature. The high quality of the quantum emission and the 1D nature of BNNTs provide potential applications in quantum technologies and hybrid optomechanics. More importantly, we achieve the fast optical modulation of the single-photon emission from the BNNTs at room temperature. The ability to control the signal from a 1D single-photon source will enable a foundation for single-photon signal processing in integrated nanophotonic systems.

†These authors contributed equally to this work.

REFERENCES

1. I. Aharonovich, D. Englund, and M. Toth, Nat. Photonics **10**, 631 (2016).
2. T. T. Tran, K. Bray, M. J. Ford, M. Toth, and I. Aharonovich, Nat. Nanotechnol. **11**, 37 (2016).
3. T. T. Tran, C. Elbadawi, D. Totonjian, C. J. Lobo, G. Grosso, H. Moon, D. R. Englund, M. J. Ford, I. Aharonovich, and M. Toth, ACS Nano **10**, 7331 (2016).
4. N. R. Jungwirth, B. Calderon, Y. Ji, M. G. Spencer, M. E. Flatté, and G. D. Fuchs, Nano Lett. **16**, 6052 (2016).
5. A. W. Schell, M. Svedendahl, and R. Quidant, "Quantum emitters in hexagonal boron nitride have spectrally tunable quantum efficiency," arXiv:1706.08303 (2017).
6. Z. Shotan, H. Jayakumar, C. R. Considine, M. Mackoit, H. Fedder, J. Wrachtrup, A. Alkauskas, M. W. Doherty, V. M. Menon, and C. A. Meriles, ACS Photon. **3**, 2490 (2016).
7. N. Chejanovsky, M. Rezai, F. Paolucci, Y. Kim, T. Rendler, W. Rouabeh, F. Fávaro de Oliveira, P. Herlinger, A. Denisenko, S. Yang, I. Gerhardt, A. Finkler, J. H. Smet, and J. Wrachtrup, Nano Lett. **16**, 7037 (2016).
8. M. Kianinia, B. Regan, S. A. Tawfik, T. T. Tran, M. J. Ford, I. Aharonovich, and M. Toth, ACS Photon. **4**, 768 (2017).
9. A. W. Schell, T. T. Tran, H. Takashima, S. Takeuchi, and I. Aharonovich, APL Photon. **1**, 091302 (2016).
10. A. Sajid, J. R. Reimers, and M. J. Ford, Phys. Rev. B **97**, 064101 (2018).
11. S. A. Tawfik, S. Ali, M. Fronzi, M. Kianinia, T. T. Tran, C. Stampfl, I. Aharonovich, M. Toth, and M. J. Ford, Nanoscale **9**, 13575 (2017).
12. X. Li, G. D. Shepard, A. Cupo, N. Camporeale, K. Shayan, Y. Luo, V. Meunier, and S. Strauf, ACS Nano **11**, 6652 (2017).
13. N. Chejanovsky, Y. Kim, A. Zappe, B. Stuhlhofer, T. Taniguchi, K. Watanabe, D. Dasari, A. Finkler, J. H. Smet, and J. Wrachtrup, Sci. Rep. **7**, 14758 (2017).
14. N. G. Chopra, R. J. Luyken, K. Cherrey, V. H. Crespi, M. L. Cohen, S. G. Louie, and A. Zettl, Science **269**, 966 (1995).
15. D. Golberg, Y. Bando, Y. Huang, T. Terao, M. Mitome, C. Tang, and C. Zhi, ACS Nano **4**, 2979 (2010).
16. Y. Lin and J. W. Connell, Nanoscale **4**, 6908 (2012).
17. X. Gao, Z.-Q. Yin, and T. Li, "High-speed quantum transducer with a single-photon emitter in an atomically thin resonator," arXiv:1712.09245 (2017).
18. G. Grosso, H. Moon, B. Lienhard, S. Ali, D. K. Efetov, M. M. Furchi, P. Jarillo-Herrero, M. J. Ford, I. Aharonovich, and D. Englund, Nat. Commun. **8**, 705 (2017).
19. M. Abdi, M.-J. Hwang, M. Aghtar, and M. B. Plenio, Phys. Rev. Lett. **119**, 233602 (2017).
20. A. L. Exarhos, D. A. Hopper, R. R. Grote, A. Alkauskas, and L. C. Bassett, ACS Nano **11**, 3328 (2017).
21. T. T. Tran, D. Wang, Z.-Q. Xu, A. Yang, M. Toth, T. W. Odom, and I. Aharonovich, Nano Lett. **17**, 2634 (2017).
22. R. V. Gorbachev, I. Riaz, R. R. Nair, R. Jalil, L. Britnell, B. D. Belle, E. W. Hill, K. S. Novoselov, K. Watanabe, T. Taniguchi, A. K. Geim, and P. Blake, Small **7**, 465 (2011).
23. C. Kurtsiefer, S. Mayer, P. Zarda, and H. Weinfurter, Phys. Rev. Lett. **85**, 290 (2000).
24. S. C. Kitson, P. Jonsson, J. G. Rarity, and P. R. Tapster, Phys. Rev. A **58**, 620 (1998).
25. J.-J. Greffet, J.-P. Hugonin, M. Besbes, N. Lai, F. Treussart, and J.-F. Roch, "Diamond particles as nanoantennas for nitrogen-vacancy color centers," arXiv:1107.0502 (2011).
26. I. Fushman, D. Englund, A. Faraon, N. Stoltz, P. Petroff, and J. Vučković, Science **320**, 769 (2008).
27. S. Weis, R. Rivière, S. Deléglise, E. Gavartin, O. Arcizet, A. Schliesser, and T. J. Kippenberg, Science **330**, 1520 (2010).
28. J. Hwang, M. Pototschnig, R. Lettow, G. Zumofen, A. Renn, S. Götzinger, and V. Sandoghdar, Nature **460**, 76 (2009).
29. M. Geiselmann, R. Marty, F. J. García de Abajo, and R. Quidant, Nat. Phys. **9**, 785 (2013).
30. M. Kianinia, C. Bradac, B. Sontheimer, F. Wang, T. T. Tran, M. Nguyen, S. Kim, Z.-Q. Xu, D. Jin, A. W. Schell, C. J. Lobo, I. Aharonovich, and M. Toth, Nat. Commun. **9**, 874 (2018).
31. Y. Liu, X. Zou, and B. I. Yakobson, ACS Nano **6**, 7053 (2012).
32. J. Storteboom, P. Dolan, S. Castelletto, X. Li, and M. Gu, Opt. Express **23**, 11327 (2015).